Int J Adv Manuf Technol (2018) 94:2679–2688
DOI 10.1007/s00170-017-1089-0

ORIGINAL ARTICLE

Research on controllability of final macroscopic specimen shape in electromagnetic superposed forming

Anlin Long[1] · **Min Wan**[1] · **Wenping Wang**[1] · **Xiangdong Wu**[1] · **Xuexi Cui**[1]

Received: 12 April 2017 / Accepted: 12 September 2017 / Published online: 16 September 2017

Abstract Electromagnetic superposed forming (EMSF) is a newly proposed method for forming large-scale aluminum alloy sheets with small curvature. The forming principle is based on superposition of local shallow deformations generated by the coaction of a flat spiral coil and a punch matrix. This paper emphasizes the deformation controllability, which is a basic research for developing the EMSF into a mature process of forming aircraft skins. The study is conducted via forming experiments in which the sheet blanks with different length-width ratio are entirely or partially subjected to the pulsed electromagnetic force. Finally, two pieces of S-shaped specimens are trail-produced. Waviness and surface finish of the specimens are analyzed. The results show that obtaining spherical specimen by EMSF is feasible. When a square blank is uniformly loaded, the specimen shape is approximately spherical. It is also feasible to obtain the major deformation perpendicular to loading paths in EMSF. The controllability of deformation during the EMSF process can be ensured. The S-shaped specimens show potential application of the EMSF in forming parts with complex shape. Besides, the specimen waviness is suitable for aircraft skins.

Keywords Electromagnetic superposed forming · Deformation controllability · Loading path · AA2524-T3 · Sheet metal · Complex shape

✉ Xiangdong Wu
wuxiangdongbuaa@163.com

[1] Department of Aircraft Manufacturing Engineering, School of Mechanical Engineering & Automation, Beihang University, Beijing 100191, People's Republic of China

1 Introduction

Electromagnetic forming (EMF) utilizes the so-called Lorentz force to form high-conductivity materials such as aluminum alloys. It is one of the high energy rate forming technologies [1]. During the forming procedure, the maximum deformation velocity of the workpiece can reach up to 50~250 m/s [2] and the high strain rate is in the range of 10^2~10^4/s [3]. Analyses of the EMF are complicated due to the highly coupled electromagnetic-mechanical-thermal fields [4–7]. When compared with traditional quasi-static forming processes, EMF will enhance the formability of metallic materials [8–12] and eliminate spring-back of workpieces [13–17]. So far, a lot of researches based on the EMF have been derived, including electromagnetic joining [18–21], cutting [22], and assisted stamping [23, 24].

Most of the successful applications are focused on compressions and expansions of tube parts. According to the published literatures, the first industrial application of EMF is the electromagnetic compression at General Motors [25]. The neoprene boots were banded onto the automotive ball joints by the electromagnetic band compression. The electromagnetically crimped form-fit joining is another application of the EMF to automotive space frame [20, 26, 27]. The outer tube is compressed into the undercut of the inner part by radial electromagnetic force. Weddeling et al. [20] claimed that the electromagnetic crimping is more energy-saving than the magnetic pulse welding and thus should be preferred in case no gas-tightness is required. Park et al. [28] have tested the connection strength. The results show that the joint failure appears in the base part but not in the joining region. Yu et al. [29] proposed the magnetic pulse cladding (MPC) in which an aluminum alloy tube is compressed onto a mild steel tube. The corrosion resistance of aluminum alloy and the mechanical strength of mild steel are gathered in the bi-metal

tube. Yu et al. [29] concluded that it is feasible to generate composite tubes with long axial length by MPC. The electromagnetic expansion is usually used to investigate the material ductility at high strain rate [30–33].

Compared with the EMF of tubular parts, the EMF of sheet metals lacks successful applications. It is thus then meaningful to take the EMF of sheet metals into further investigation. Non-uniform distribution of electromagnetic force of flat spiral coil is a limitation for EMF of sheets. In order to enhance the spatial distribution of magnetic pressure, Kamal et al. [34] introduced a uniform pressure coil. The coil was then used to trail-produce shell of cellphone [35] and bipolar plate of fuel cell [36]. Usually, the electromagnetic free bulging is used to test formability of sheet metals at high strain rate. The traditional rigid punch is substituted by pulsed electromagnetic force. It is a single-die process which eliminates the effect of fraction on testing formability of materials.

Aircraft skins which are made of aluminum alloys are typical sheet metals. Recently, a novel forming method aimed at manufacturing large-scale and small-curvature aircraft skins has been proposed [37, 38]. It is named electromagnetic superposed forming (EMSF). As is shown in Fig. 1, local shallow deformations are generated by coaction of electromagnetic driving and punch matrix restraining. After spring-back, superposition of these local deformations leads to macroscopic shape of specimen. The experiments conducted by Long et al. [37] have shown the feasibility of the EMSF. The specimens will bend towards opposite directions by different combinations of discharge voltage and rubber thickness. Based on the EMSF method, a large-scale AA2524-T3 blank with a size of 1840 mm × 810 mm × 2.5 mm has been formed to be a 1D curved sheet specimen [38]. The average radius of that specimen was approximately 6200 mm. The authors concluded that the new EMSF process might be suited for forming aircraft skins.

Because local deformations are approximately spherical, the specimen may get 2D curved. When a square blank is uniformly loaded, the specimen shape might be approximately spherical. It is similar to the deformation law observed in the free shot peen forming. However, the desired shape of parts is not always spherical or even two-dimensional curved. For example, a lot of S-shaped aircraft skins are needed to meet the requirements of blended wing body configuration and twin-engine design of aircraft. The so-called S-shape is defined from the geometric point of view. When a line or a curve is moved along a given path, a new 3D surface with certain shape will be created. The line or curve is called the generatrix, and the path is called the directrix. The S-shape geometry means that the directrix of the surface is S-shaped, which looks like a cubic curve. The principal curvature in the directrix is much larger than the other one in the generatrix. For an S-shaped specimen, the major deformation is formed along the directrix.

The EMSF process is expected to be a new approach for producing aircraft skins. It is necessary to take an insight into the controllability of final macroscopic shape of specimen in the EMSF process. Because the electromagnetic forces are incrementally applied on the sheet surface during EMSF procedure, effect of loading path on final deformation of specimen should be taken into consideration. Referring to the well-known shot peening, it is expected that the maximum principal curvature appears in the direction perpendicular to the loading path. The sphere effect in EMSF could be inhibited, which makes it easy to control the final shape of parts.

This work starts with a verification of the feasibility of EMSF in forming dome-shaped specimens. Next, the experiments inhibiting the sphere effect of macroscopic specimen deformation are carried out. As an application of the deformation controllability, the S-shaped sheet specimens with large scale are then trial-produced by EMSF. All of the sheet blanks are made of 2524-T3 aluminum alloys. Analyses of the specimens are assisted by a three-dimensional laser scanner and the commercial software CATIA.

2 Experiments

2.1 Experimental tools

A flat spiral coil that can be lifted by a hydraulic cylinder is utilized to generate the pulsed electromagnetic force. It consists of 15 turns and has a cross section of 16 mm × 2.5 mm. The insulation gaps between every two adjacent turns is 0.5 mm. The punch matrix consists of 162 (27 × 6) punches (see Fig. 2). Discharging energy of the coil is supplied by a capacitor bank with 250 μF capacitance. The maximum charge voltage of the capacitor bank is 20 kV.

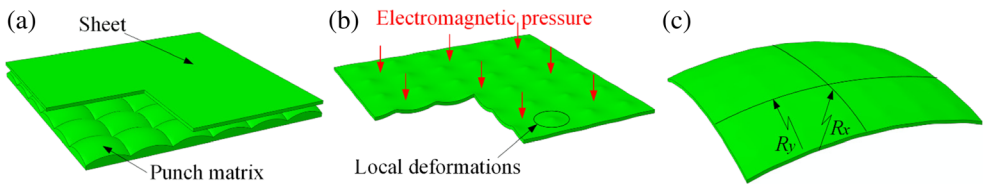

Fig. 1 Schematic diagram of the electromagnetic superposed forming (EMSF) procedure. **a** The sheet is placed above a punch matrix which consists of regularly arranged punches with spherical end. **b** Applying electromagnetic force on that sheet results in uniformly distributed local shallow spherical deformations. **c** Superposition of these local deformations leads to macroscopic deformation of the specimen

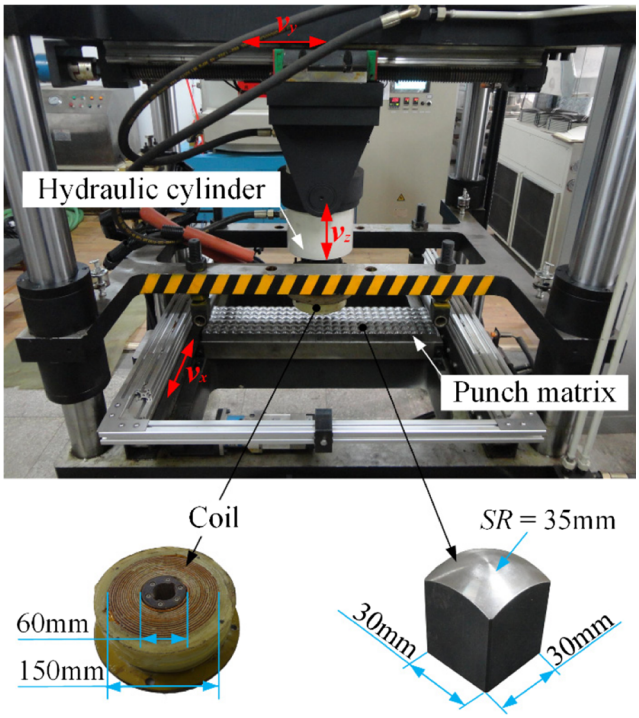

Fig. 2 Demonstration of the experimental tools

2.2 Forming dome-shaped specimen

According to spherical punch end, local deformations generated in EMSF are also approximately spherical. A square blank might get macroscopic spherical deformation in case that the local deformations are uniformly distributed. This experiment is aimed at experimentally verifying the feasibility of obtaining a dome-shaped specimen by the EMSF. Figure 3a shows the experimental setup. The rubber sheets are used to prevent the specimen surface from mechanical fraction. A polyurethane sheet is placed between the coil and the driver sheet. Both the driver sheet and specimen sheet are in size of 550 mm × 330 mm × 1.6 mm. Figure 3b shows the loading procedures. The specimen is firstly loaded along its length direction. For every two adjacent work stations in one loading path, the feeding distance is set to 30 mm. The distance between every two adjacent paths is 30 mm too. A total of 36 discharging has been carried out, and the middle zone of the specimen which is in the range of 300 mm × 300 mm has been loaded. The discharging voltage for the coil at every work station is set to 4 kV.

2.3 Inhibiting sphere effect

As the desired shape of parts is not always spherical, the following experiments are aimed at inhibiting the spherical deformation of specimens during EMSF. Figure 4a shows the experimental setup. The rubber and polyurethane sheets are similar to the above experiment (see Sect. 2.2). The size of the

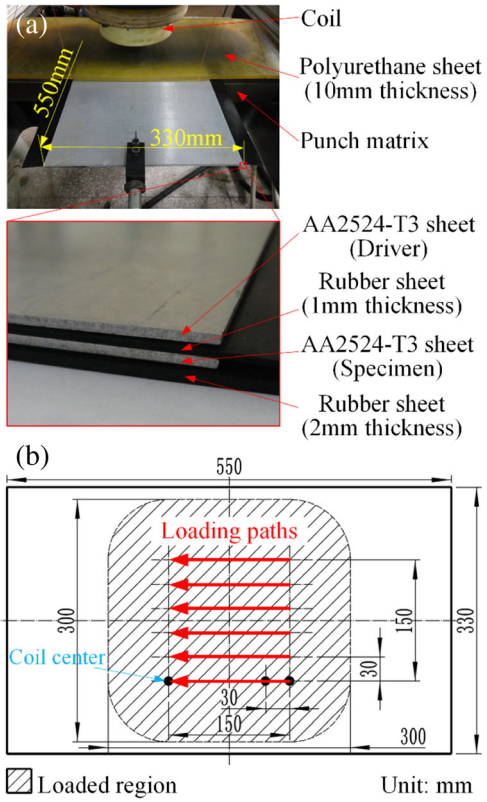

Fig. 3 **a** Experimental setup and **b** loading procedures in the forming of dome-shaped specimens

driver sheet is in the range of 810 mm × 200 mm × 1.6 mm. Figure 4b presents a more detailed illustration of the loading procedure. The length and thickness of the specimens are 810 and 1.6 mm, respectively. The width of the specimens, *B*,

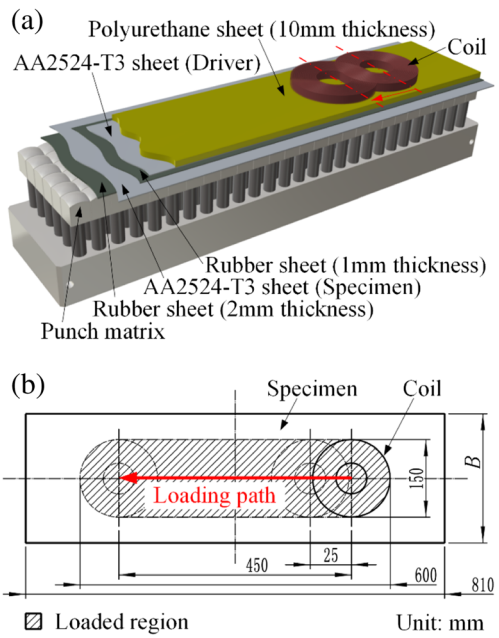

Fig. 4 **a** Experimental setup and **b** loading procedure for inhibiting sphere effect

varies from 150 to 350 mm with a 50-mm increment. The minimum width equals to the effective outer diameter of the coil (see Fig. 2). A total of five specimens are formed by the EMSF process. The feeding distance of the coil between every two adjacent work stations is set to 25 mm, and the total displacement of the coil center is 450 mm. The discharging voltage of the capacitor bank is 4 kV. Referring to Fig. 4b, it should be noticed that the specimens are partially loaded and the undeformed region at both ends of the specimens will be trimmed off in the following analysis (see Sect. 3.2).

2.4 Forming S-shaped specimens

The S-shaped aircraft skin is a representative of aircraft skins with complex geometry. It is meaningful to carry out the forming experiments of the S-shaped specimens by the EMSF process. A brief introduction of the experimental setup is shown in Fig. 5a. Thickness of the AA2524-T3 blank is 2.5 mm. It is closer to the thickness of general aircraft skins. The rubber and polyurethane sheets are in 2 and 10 mm thickness, respectively. In order to obtain an S-shaped deformation, the left half of the specimen is loaded from the upper side while the other half is loaded from the lower side (see Fig. 5b). For the S-shaped specimen 1 and specimen 2, discharging voltages at every work station are 4.5 and 5 kV, respectively.

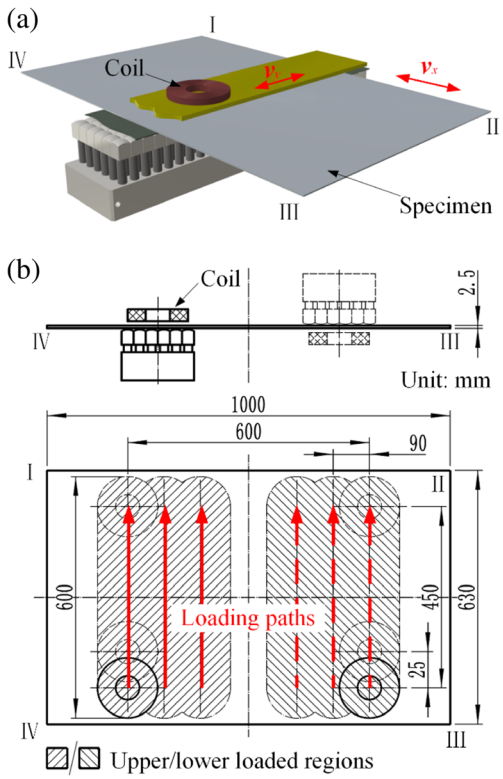

Fig. 5 **a** Experimental setup and **b** loading procedures in the forming of S-shaped specimen

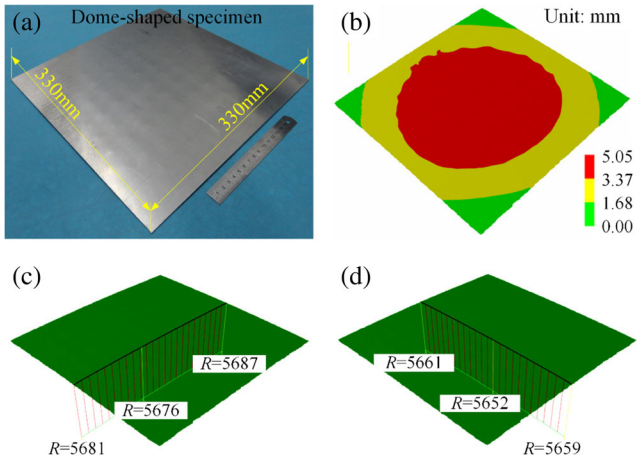

Fig. 6 **a** Photograph, **b** deflection contour, and **c**, **d** curvature radii of the dome-shaped specimen

3 Results and discussions

3.1 Dome-shaped specimen

According to the forming procedure (see Fig. 3), local deformation appears in the middle part of the sheet blank. It is in the range of 330 mm × 330 mm. Therefore, the undeformed clamping allowances were trimmed off and the dome-shaped specimen is shown in Fig. 6a. In order to get more detailed geometric information, the specimens were scanned by a three-dimensional laser scanner, which outputs cloud-point data. The data was then analyzed by the commercial software CATIA using the Deviation Analysis Function. The deflection contour of the dome-shaped specimen is plotted in Fig. 6b. The maximum deflection is 5.05 mm. For curvature radius analysis, two quadratic curves are fitted (see Fig. 6c, d). The curvature radii in both directions are approximately equal to each other, and the average spherical radius is approximately 5669 mm. Both the deflection contour and the curvature radius show that the formed specimen is approximately spherical. Therefore, it could be concluded that making a square blank, which is uniformly loaded by the EMSF process, into a dome-shaped specimen is feasible.

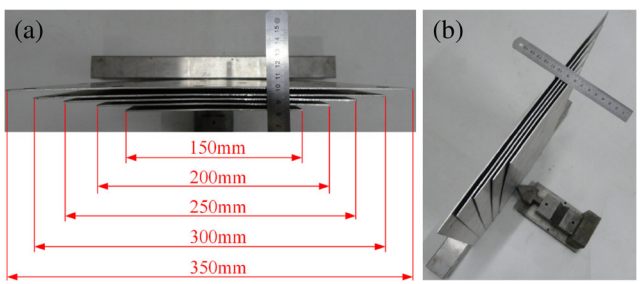

Fig. 7 **a** Top and **b** axonometric views of the specimens obtained in sphere effect inhibition experiments

3.2 Sphere effect inhibition

Because the aircraft skins are not always spherical or even two-dimensional curved, the sphere effect of specimen deformation should be inhibited. Obtaining the major deformation in the direction perpendicular to the loading path is conducive to controlling the macroscopic shape of the specimen during the EMSF process. Figure 7 shows the photographs of the specimens formed in the sphere effect inhibition experiments (see Sect. 2.3). Clamping allowances of the specimens at both ends were trimmed off. Only the deformed middle parts in 480 mm length are taken into consideration in the following analyses.

Deformation of the specimens is characterized by geometric parameters, as is shown in Fig. 8. The deflection contour line is elliptical due to the sphere effect of specimen. Lengths of the major and minor axes of the ellipse are presented by D_a and D_b, respectively. The distance between contour plane and surface peak is H. Therefore, the principal curvature radii R_x and R_y at that peak are expressed as

$$\begin{cases} R_x = \dfrac{D_b^2 + 4H^2}{8H} \\ R_y = \dfrac{D_a^2 + 4H^2}{8H} \end{cases} \quad (1)$$

Deformation analysis of the specimens is based on the relative relationship between R_x and R_y. The major deformation of specimen is in accordance with the minimum principal curvature radius.

Importing the point-cloud data of the specimens scanned by a three-dimensional laser scanner into commercial software CATIA, deflection contours are obtained by the Deviation Analysis Function. The deflection contours as well as length of the major and minor ellipse axes are shown in Fig. 9.

According to the above deflection contours, the ratio of D_b to D_a and the principal curvature radius of each specimen are plotted in Figs. 10 and 11. The ratio decreases with increment of specimen width while the maximum principal curvature radius R_y increases with increment of specimen width. Variation of the minimum principal curvature radius is not obvious when compared with the maximum one. It should be noticed that R_x and R_y are approximately equal to the curvature radius of the specimen in width and length directions, respectively. Therefore, the results show that increasing

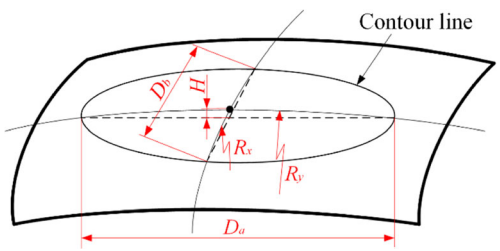

Fig. 8 Illustration of the specimen deformation analysis

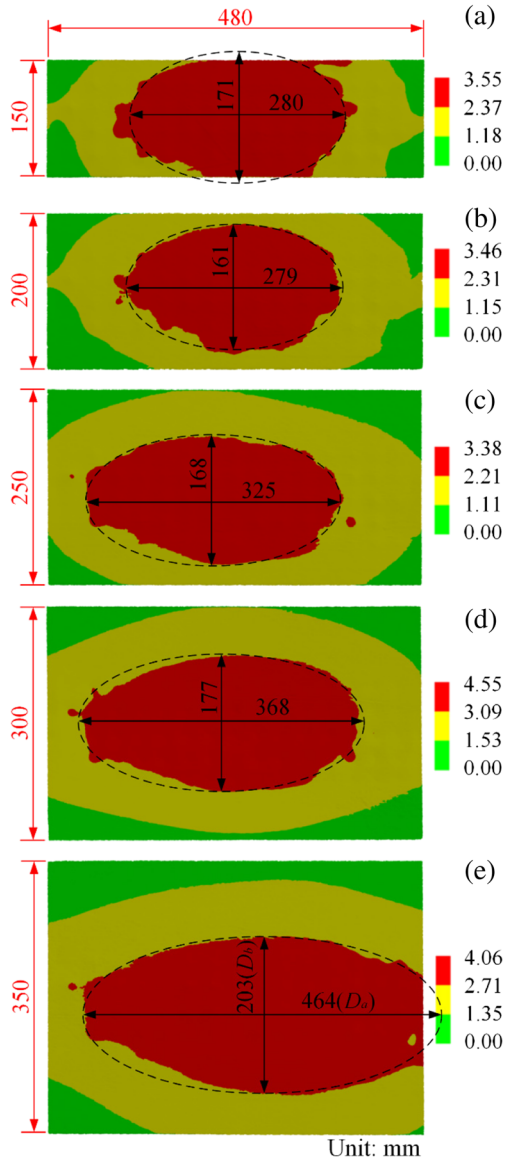

Fig. 9 **a**–**e** Deflection contours of the specimens obtained in sphere effect inhibition experiments

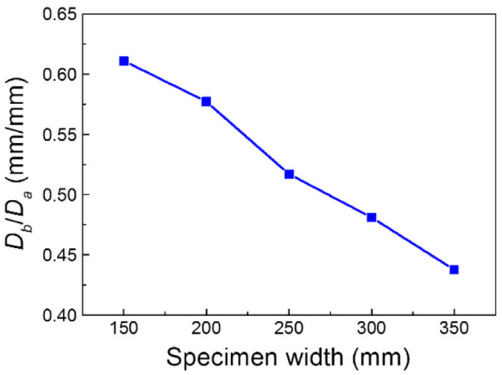

Fig. 10 Ratio of D_b to D_a versus width of specimens obtained in sphere effect inhibition experiments

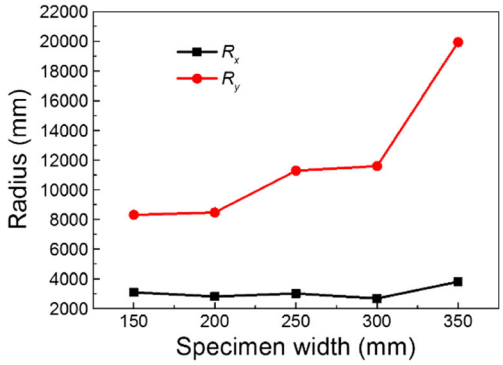

Fig. 11 Variations of the principal curvature radius of specimens obtained in sphere effect inhibition experiments

the specimen width will inhibit the sphere effect. The major deformation is obtained in the direction perpendicular to the loading path (refer to Fig. 4).

A qualitative illustration of the inhibiting principle is presented by a specimen which is partially loaded in the length direction, as is shown in Fig. 12a. If the specimen is imaginarily cut open (Fig. 12b), the loaded region will get vaulted. The principal curvature radii, R_x and R_y, are close to each other. In fact, bending of the loaded region in length direction is restrained by the unloaded region via the internal shear forces along the imaginary boundaries. It enlarges the principal curvature radius R_y and results in major deformation in the direction perpendicular to the loading path.

3.3 S-shaped specimens

3.3.1 Deflection

Two S-shaped specimens were obtained in this work, and photographs of these specimens are presented in Fig. 13. Restrained by the spherical ends of punches, local shallow

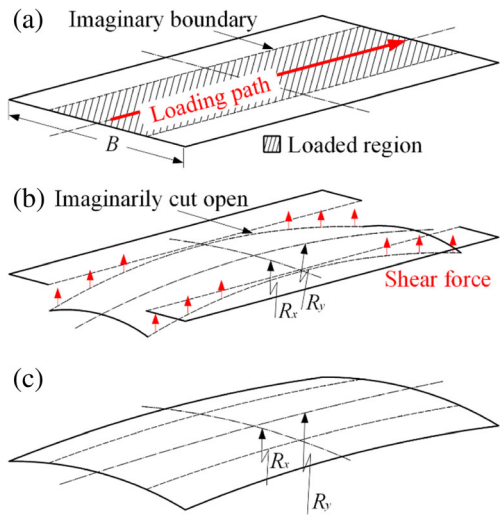

Fig. 12 **a**–**c** Schematic diagram of the principle for obtaining the major deformation in the direction perpendicular to the loading path

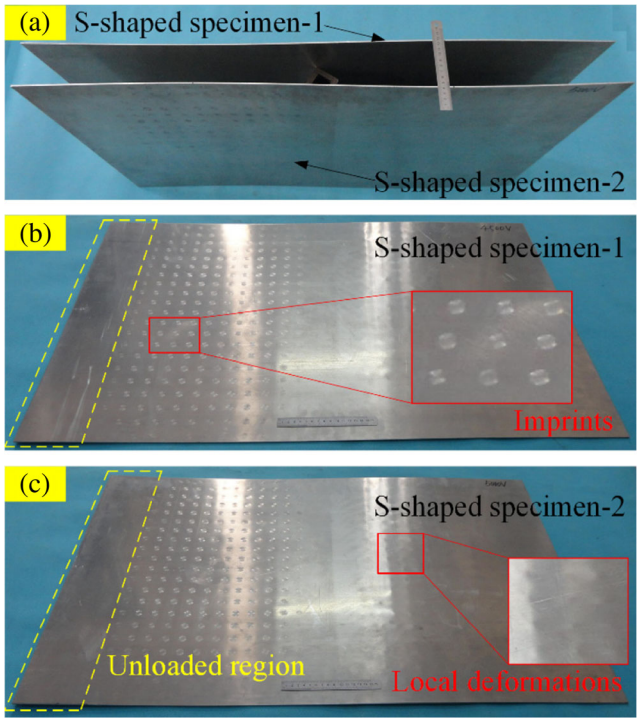

Fig. 13 **a** Side and **b**, **c** top views of the S-shaped specimens

deformations can be observed in case of careful observation (see Fig. 13c). Again scanned by the 3D laser scanner, deformation contours of the S-shaped specimens are shown in Fig. 14. Obviously, under the combined action of the restriction of unloaded regions and the mutual restriction of each other's side, the major curling appears in the direction perpendicular to loading paths (see Fig. 5). The specimens are approximately rotationally symmetric. The curved contour lines mean that these S-shaped specimens are also slightly two-dimensional curved. When compared with specimen scale, the magnitude of the S-shaped deformation is much smaller.

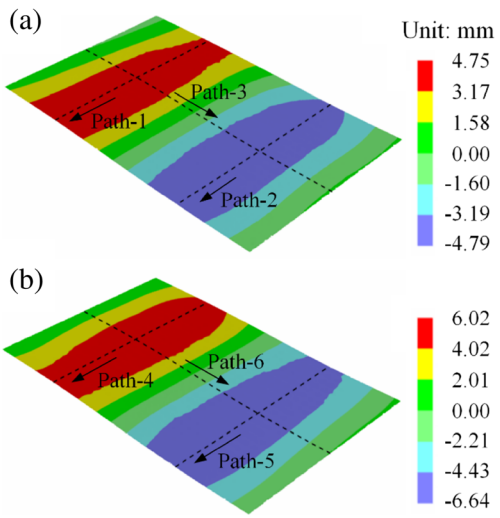

Fig. 14 Deflection contours of the S-shaped (**a**) specimen 1 and (**b**) specimen 2

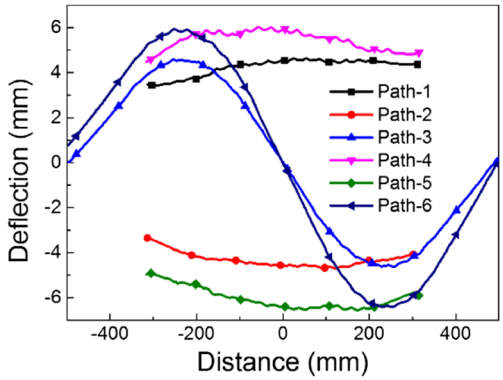

Fig. 15 Variation of the deflection of the S-shaped specimens along different paths

Therefore, six paths are defined in Fig. 14 for a clear observation of the specimen deflection, as is shown in Fig. 15. Comparison of the specimen maximum deflection shows that the deflection of specimen increases with the increasing of capacitor discharging voltage.

3.3.2 Curvature

Based on the extracted paths, six curves are fitted by polynomial functions for analysis of specimen curvature. Figure 16 shows the variation of the curve curvature. These curves are in accordance with the paths defined in Fig. 14. The curvatures are carried out using the Porcupine Curvature Analysis function of the commercial software CATIA. Length of the comb represents the relative magnitude of curvature at that point. Some extremum values are also presented. The figures show that the specimen curvature in the direction perpendicular to loading paths (see Fig. 5) is much bigger than the transverse curvature along loading paths. It is verified that the S-shaped specimens are two-dimensional curved. In electromagnetic superposed forming using the punch matrix with flat envelope (see Fig. 2), the sphere effect of specimen can be inhibited but not eliminated. The average maximum curvature for S-shaped specimen 1 and specimen 2 are respectively 1.969×10^{-4} and 2.561×10^{-4}/mm, namely, the average minimum radii are approximately 5079 and 3905 mm. According to length of the combs, the curvature increases with the increasing of discharging voltage.

3.3.3 Waviness

Waviness of the specimen, δ, is defined as

$$\delta = \frac{d}{l} \tag{2}$$

where d is the amplitude of wave and l is the wavelength, as is shown in Fig. 17a. It is a dimensionless quantity. Because distribution of local deformations is in accordance with punch matrix, the wavelength equals to the distance between every two adjacent punch axes, i.e., 30 mm. Amplitude measurement is conducted using a curvature device of which the resolution is 0.005 mm (see Fig. 17b).

Measuring the wave amplitude and calculating waviness at every local deformation, waviness contours of the S-shaped specimens are shown in Fig. 18. The maximum waviness of specimen 1 and specimen 2 are 0.00384 and 0.008, respectively. Correspondingly, the maximum wave amplitudes are 0.115 and 0.24 mm. The average waviness of the loaded region of S-shaped specimen 1 and specimen 2 is 0.00184 and 0.00252, respectively. According to the Aviation Industry Standard of People's Republic of China (HB 7086-94, in Chinese), both waviness and amplitude of the local residual deformations of the S-shaped specimens meet the requirements of fuselage skins of aircraft whose cruising speed is in the range of 300 to 600 km/h.

For practical industrial applications, it is expected that the waviness should be as small as possible and the superposed macroscopic deformation should be as large as possible. Comparing the average waviness of each specimen, it is indicated that specimen waviness decreases with decreasing

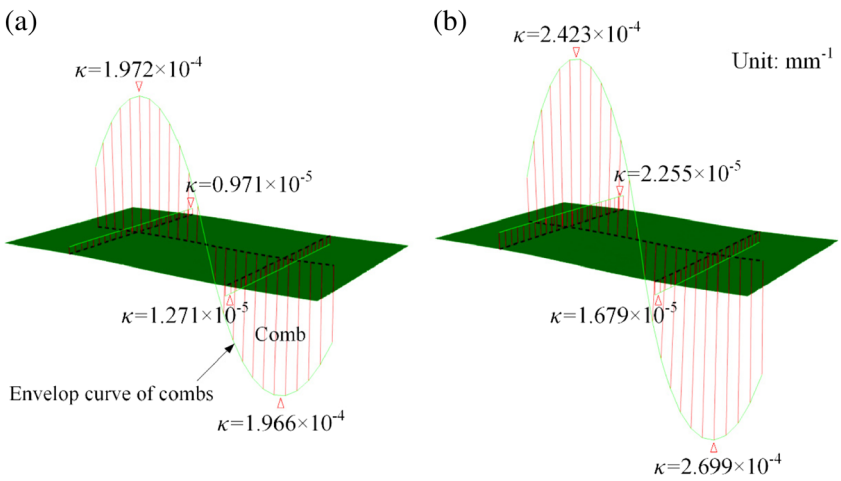

Fig. 16 Demonstration of the curvature of the S-shaped (**a**) specimen 1 and (**b**) specimen 2

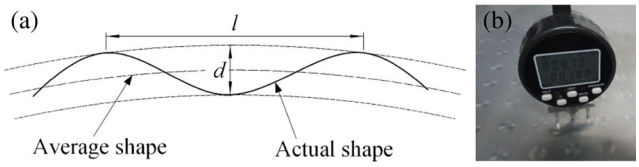

Fig. 17 **a** Illustration of specimen waviness. **b** Measurement of the amplitude

discharging voltage. The above Sects. 3.3.1 and 3.3.2 show that the macroscopic deformation of specimen increases with increment of discharging voltage. Therefore, in case that the other process parameters remain unchanged, this contradiction can only be moderated but not solved by changing the discharging voltage. For future researches, effects of rubber sheet thickness, local deformation distribution, and specimen thickness on this contradiction should be taken into consideration. It may result in good comprehensive performance of this newly proposed EMSF process.

3.3.4 Surface finish

Although the specimens are separated from the punch matrix by rubber sheet, the imprints appear on the specimen surface adjacent to punches (Fig. 13b). Besides, the collision between the large-scale blank and experimental tools is unavoidable during the forming procedure, which makes the specimen surface scratched. Given importance of the surface finish, one surface of each specimen has been painted with army green, as is shown in Fig. 19. The target points attached to the unpainted surface are used for the above-mentioned surface scan (refer to Sect. 3.3.1). Comparisons of surface finish between the unpainted and painted surfaces of each specimen show

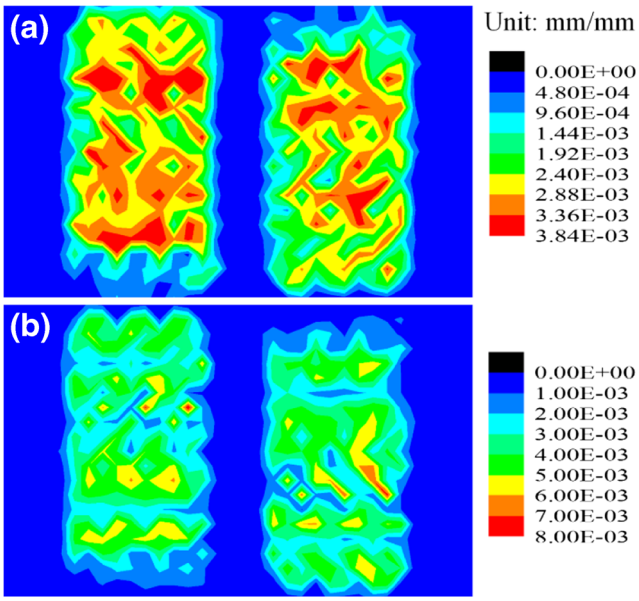

Fig. 18 Waviness contours of the S-shaped (**a**) specimen 1 and (**b**) specimen 2

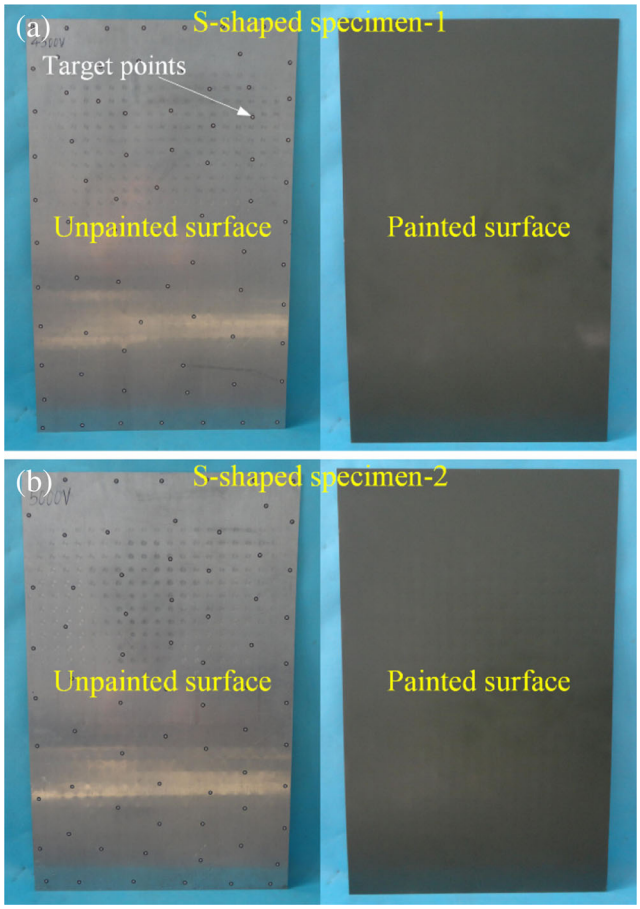

Fig. 19 Comparisons of the surface finish of the S-shaped (**a**) specimen 1 and (**b**) specimen 2

that the imprints and/or the scratches can be eliminated by painting. Therefore, the surface finish of the specimens formed by the EMSF process could be ensured, which makes the EMSF process meet the basic requirement of an industrial application.

4 Conclusions

This paper emphasizes the controllability of final macroscopic specimen shape in EMSF. It is aimed at developing a new forming technology for manufacturing large-scale specimens with small curvature and deformation. Based on the experimental results and discussions, the following conclusions can be drawn:

1. Local deformations are approximately spherical due to the spherical punch end in EMSF, which results in macroscopically two-dimensional curved specimen after spring-back. Obtaining spherical dome-shaped specimens by the EMSF process is feasible if a square blank is

uniformly loaded. The average spherical radius of the formed specimen in this work is approximately 5669 mm.
2. When the specimen is partially loaded, the undeformed region will inhibit the superposition of local deformations. Therefore, inhibiting the sphere effect and obtaining the major deformation in the direction perpendicular to loading paths are feasible. The controllability of the deformation during the EMSF process can be ensured. However, the sphere effect can be inhibited but not completely eliminated.
3. Deformation controllability of the EMSF process is applied to forming the S-shaped specimens. The ability of the EMSF process in manufacturing specimen with complex geometric shape is verified. The average minimum radius of the obtained S-shaped specimens varies from 3905 to 5079 mm. Waviness and amplitude of the local residual deformations meet the requirements of fuselage skins of aircraft.

For future researches, effect of residual stress on industrial application of the EMSF process should be taken into consideration. Reducing the specimen waviness and enlarging the specimen deflection by optimizing process parameters should also be investigated.

Acknowledgements This work was supported by the National Basic Research Program of China (973 Program, Grant No. 2011CB012804) and the Excellence Foundation of BUAA for PhD Students (Grant No. 2017046). The authors wish to acknowledge assistances of these programs for the financial support.

References

1. Psyk V, Risch D, Kinsey BL, Tekkaya AE, Kleiner M (2011) Electromagnetic forming—a review. J Mater Process Technol 211:787–829. https://doi.org/10.1016/j.jmatprotec.2010.12.012
2. Mamalis AG, Manolakos DE, Kladas AG, Koumoutsos AK (2004) Electromagnetic forming and powder processing: trends and developments. Appl Mech Rev 57(4):299. https://doi.org/10.1115/1.1760766
3. Daehn GS, Zhang Y, Golowin S, Banik K, Vivek A, Johnson JR, Taber G, Fenton GK, Henchi I, L'Eplattenier P (2008) Coupling experiment and simulation in electromagnetic forming using photon doppler velocimetry. Paper presented at the 3rd International Conference on High Speed Forming, Dortmund
4. Stiemer M, Unger J, Blum H, Svendsen B (2006) Fully-coupled 3D simulation of electromagnetic forming. Paper presented at the 2nd International Conference on High Speed Forming, Dortmund
5. Wang L, Chen ZY, Li CX, Huang SY (2006) Numerical simulation of the electromagnetic sheet metal bulging process. Int J Adv Manuf Technol 30:395–400. https://doi.org/10.1007/s00170-005-0094-x
6. L'Eplattenier P, Cook G, Ashcraft C, Burger M, Imbert J, Worswick M (2009) Introduction of an electromagnetism module in LS-DYNA for coupled mechanical-thermal-electromagnetic simulations. Steel Res Int 80(5):351–358. https://doi.org/10.2374/sri08sp152
7. Cao Q, Li L, Lai Z, Zhou Z, Xiong Q, Zhang X, Han X (2014) Dynamic analysis of electromagnetic sheet metal forming process using finite element method. Int J Adv Manuf Technol 74:361–368. https://doi.org/10.1007/s00170-014-5939-8
8. Seth M, Vohnout VJ, Daehn GS (2005) Formability of steel sheet in high velocity impact. J Mater Process Technol 168:390–400. https://doi.org/10.1016/j.jmatprotec.2004.08.032
9. Golovashchenko SF (2007) Material formability and coil design in electromagnetic forming. J Mater Eng Perform 16:314–320. https://doi.org/10.1007/s11665-007-9058-7
10. Xu J, Yu H, Cui J, Li C (2013) Formability of AZ31 magnesium alloy sheets during magnetic pulse bulging. Mater Sci Eng A 569:150–158. https://doi.org/10.1016/j.msea.2013.01.016
11. Li F, Mo J, Li J, Huang L, Zhou H (2013) Formability of Ti–6Al–4V titanium alloy sheet in magnetic pulse bulging. Mater Des 52:337–344. https://doi.org/10.1016/j.matdes.2013.05.064
12. Li F, Mo J, Li J, Zhao J (2016) Formability evaluation for low conductive sheet metal by novel specimen design in electromagnetic forming. Int J Adv Manuf Technol 88:1677–1685. https://doi.org/10.1007/s00170-016-8893-9
13. Golovashchenko SF (2005) Springback calibration using pulsed electromagnetic field. In: Smith LM (ed) Numisheet 2005, pp 284–285. https://doi.org/10.1063/1.2011234
14. Iriondo E, Gonzalez B, Gutierrez M, Vonhout V, Daehn G, Hayes B 2006 Electromagnetic springback reshaping. In: 2nd International Conference on High Speed Forming
15. Iriondo E, Gutiérrez MA, González B, Alcaraz JL, Daehn GS (2011) Electromagnetic impulse calibration of high strength sheet metal structures. J Mater Process Technol 211:909–915. https://doi.org/10.1016/j.jmatprotec.2010.05.013
16. Woodward S, Weddeling C, Daehn G, Psyk V, Carson B, Tekkaya AE (2011) Production of low-volume aviation components using disposable electromagnetic actuators. J Mater Process Technol 211:886–895. https://doi.org/10.1016/j.jmatprotec.2010.07.020
17. Iriondo E, Alcaraz JL, Daehn GS, Gutiérrez MA, Jimbert P (2013) Shape calibration of high strength metal sheets by electromagnetic forming. J Manuf Process 15:183–193. https://doi.org/10.1016/j.jmapro.2013.01.007
18. Deng JH, Yu HP, Li CF (2009) Numerical and experimental investigation of electromagnetic riveting. Mater Sci Eng A 499:242–247. https://doi.org/10.1016/j.msea.2008.05.049
19. Kapil A, Sharma A (2015) Magnetic pulse welding: an efficient and environmentally friendly multi-material joining technique. J Clean Prod 100:35–58. https://doi.org/10.1016/j.jclepro.2015.03.042
20. Weddeling C, Walter V, Haupt P, Tekkaya AE, Schulze V, Weidenmann KA (2015) Joining zone design for electromagnetically crimped connections. J Mater Process Technol 225:240–261. https://doi.org/10.1016/j.jmatprotec.2015.06.009
21. Yu H, Tong Y (2016) Magnetic pulse welding of aluminum to steel using uniform pressure electromagnetic actuator. Int J Adv Manuf Technol. https://doi.org/10.1007/s00170-016-9928-y
22. Maier-Komor P, Hoffmann H, Ostermair M (2010) Cutting of hollow profiles using electromagnetic fields. Int J Mater Form 3(S1):503–506. https://doi.org/10.1007/s12289-010-0817-x
23. Okoye CN, Jiang JH, Hu ZD (2006) Application of electromagnetic-assisted stamping (EMAS) technique in incremental sheet metal forming. Int J Mach Tool Manu 46:1248–1252. https://doi.org/10.1016/j.ijmachtools.2006.01.029
24. Choi MK, Huh H, Park N (2017) Process design of combined deep drawing and electromagnetic sharp edge forming of DP980 steel sheet. J Mater Process Technol 244:331–343. https://doi.org/10.1016/j.jmatprotec.2017.01.035
25. Zittel G (2010) A historical review of high speed metal forming. Paper presented at the 4th International Conference on High Speed Forming

26. Weddeling C, Woodward ST, Marré M, Nellesen J, Psyk V, Tekkaya AE, Tillmann W (2011) Influence of groove characteristics on strength of form-fit joints. J Mater Process Technol 211(5): 925–935. https://doi.org/10.1016/j.jmatprotec.2010.08.004
27. Eguia I, Zhang P, Daehn GS (2004) Improved crimp-joining of aluminum tubes onto mandrels with undulating surfaces. Paper presented at the 1st International Conference on High Speed Forming, Dortmund
28. Park YB, Kim HY, Oh SI (2005) Design of axial/torque joint made by electromagnetic forming. Thin-Walled Struct 43:826–844. https://doi.org/10.1016/j.tws.2004.10.009
29. Yu H, Fan Z, Li C (2014) Magnetic pulse cladding of aluminum alloy on mild steel tube. J Mater Process Technol 214:141–150. https://doi.org/10.1016/j.jmatprotec.2013.08.013
30. Tamhane A, Altynova MM, Daehn GS (1996) Effect of sample size on ductility in electromagnetic ring expansion. Scr Mater 34(8): 1345–1350
31. Altynova M, Hu X, Daehn GS (1996) Increased ductility in high velocity electromagnetic ring expansion. Metall Mater Trans A 27A:1837–1844. https://doi.org/10.1007/bf02651933
32. Thomas JD, Triantafyllidis N (2007) Theory of necking localization in unconstrained electromagnetic expansion of thin sheets. Int J Solids Struct 44:6744–6767. https://doi.org/10.1016/j.ijsolstr.2007.03.007
33. Shin C, Jin HH, Lee JG (2008) Expansion of a low conductive metal tube by an electromagnetic forming process: finite element modeling. Met Mater Int 14(1):91–97. https://doi.org/10.3365/met.mat.2008.02.091
34. Kamal M, Daehn GS (2007) A uniform pressure electromagnetic actuator for forming flat sheets. J Manuf Sci Eng 129(2):369. https://doi.org/10.1115/1.2515481
35. Kamal M, Shang J, Cheng V, Hatkevich S, Daehn GS (2007) Agile manufacturing of a micro-embossed case by a two-step electromagnetic forming process. J Mater Process Technol 190(1–3):41–50. https://doi.org/10.1016/j.jmatprotec.2007.03.114
36. Kamal M, Cheng V, Bradley J, Hatkevich S, Daehn GS (2006) Design, construction, and applications of the uniform pressure electromagnetic actuator. Paper presented at the 2nd International Conference on High Speed Forming, Dortmund
37. Long A, Wang W, Fang C, Wu X, Wan M (2016) A novel forming method of aluminum sheet based on superposition principle of electromagnetic local forming. J Phys Conf Ser 734(3):032002. https://doi.org/10.1088/1742-6596/734/3/032002
38. Long A, Wan M, Wang W, Wu X, Cui X, Fang C (2017) Electromagnetic superposed forming of large-scale one-dimensional curved AA2524-T3 sheet specimen. Int J Adv Manuf Technol. https://doi.org/10.1007/s00170-017-0127-2